



# Projected changes in heat wave characteristics over India

Neethu C<sup>1,2</sup> · K V Ramesh<sup>1</sup>

Published online: 12 October 2023  
© The Author(s), under exclusive licence to Springer Nature B.V. 2023

## Abstract

Heat waves (HW) are increasing in intensity, frequency, and duration. The projected changes in the characteristics of HW at the regional level are essential input to develop mitigation strategies to minimize social risks in densely populated regions. In this study, we examine the projected spatiotemporal changes in heat wave characteristics under different climate change scenarios using simulations of Coupled Model Intercomparison Project phase 6 (CMIP6) in seven temperature homogeneous zones of India, i.e., North West (NW), North Central (NC), West Coast (WC), East Coast (EC), Interior Peninsula (IP), Western Himalaya (WH) and North East (NE). The results show that the area of occurrence of a daily maximum temperature above 43°C is projected to increase about 16-fold over WC, 10-fold over EC, and in other zones in the range of 1-3 fold. The warm days are projected to increase fivefold over WC and threefold over NW, EC, IP, and WH. In India, HW days are projected to increase by 7-8 days in the near future (2025-2050) and by 10-17 days in the far future (2076-2100), while under SSP585 over WH (24 days), NW (19 days), and other zones 12-15 days in the far future. EC and WC are plausible to be more vulnerable under SSP370 and SSP585, with an increase in HW intensity (>1.5°C). The area of occurrence of long-lasting heat waves over WC is expected to have a drastic increase of more than 20-fold under all scenarios, while increasing 12-fold over IP and 8-fold over NC, EC, and WH under SSP585. The projected HW days will be more intense in the coastal zones and more frequent over WH and NW.

**Keywords** Heat waves · Climate scenarios · Extreme temperature · CMIP6

## 1 Introduction

Heat waves (HW) are prolonged periods of anomalous surface air temperature, and their intensity, frequency, and duration have been increasing since 1950 (Perkins-Kirkpatrick and

---

✉ K V Ramesh  
kvram55@gmail.com  
Neethu C  
44neethu@gmail.com

<sup>1</sup> Earth and Engineering Sciences Division, CSIR Fourth Paradigm Institute, Bengaluru, Karnataka, India

<sup>2</sup> Visvesvaraya Technological University, Belagavi, Karnataka, India

Lewis 2020). HW will inflict disastrous impacts on human health, agriculture, infrastructure, water resources, and the livelihood of millions of people (Lu and Kueppers 2015; Chakraborty et al. 2019). Heat waves are one of the deadliest natural hazards in many geographical locations like Australia (Coates et al. 2014), Europe (Mitchell et al. 2016), the US (Anderson and Bell 2011) and India (Ray et al. 2021). An increase in global surface air temperature will intensify climate extremes such as heat waves, floods, and drought (Perkins et al. 2012; Ali et al. 2019; Spinoni and et al. 2020). Anthropogenic climate change is the main contributor to the increasing trends observed in HW (Stott et al. 2004). Mazdiyasi et al. (2017) have shown that a practically unavoidable moderate increase in mean temperature by  $0.5^{\circ}\text{C}$  itself will increase heat-related mortality. Intergovernmental Panel on Climate Change (IPCC) Sixth Assessment Report (AR6) shows that global surface air temperature has increased by  $0.85^{\circ}\text{C}$  from 1850-1900 (base period) to 1995-2014, but the increase from the base period to 2011-2020 is  $1.09^{\circ}\text{C}$  (Delmotte et al. 2021). During the near term (2020-2041) global surface air temperature will be increasing by  $1.5^{\circ}\text{C}$  (Delmotte et al. 2021), which will affect 790 million people in South Asia (Aadhar and Mishra 2019). By the end of 2100, the exposure of the global population to extreme heat will increase 30 times (Liu et al. 2017).

Heat waves over India occur mostly during April-June; during this period, the temperature anomalies will be at their peak (Ratnam et al. 2016; Neethu et al. 2020). Observational studies show a significant increase in all India mean annual temperature during recent decades (Kothawale and Rupa Kumar 2005; Panda et al. 2017; Ross et al. 2018). During the 1950s, limited areas had temperatures reaching a maximum of  $40^{\circ}\text{C}$ , but by the 2010s, the area experiencing temperatures surpassing  $40^{\circ}\text{C}$  had expanded to most of the Indian peninsula (Ross et al. 2018). The heat wave prone regions of India are the Indo-Gangetic plains, North West India, and over states like Andhra Pradesh and Odisha (Neethu and Ramesh 2022; Mandal et al. 2019; Pattanaik et al. 2017). Heat waves are strongly related to the tropical SST variations of the Pacific (Hari et al. 2022), the Bay of Bengal (Jenamani and Jendrakumar 2012), and the Atlantic (Vittal et al. 2020). Over India, heat wave variability is closely connected with El Niño Southern Oscillation (ENSO) (Rohini et al. 2019; Murari et al. 2016; Ratnam et al. 2016). Extended and intense Indian heat waves occur mostly during the succeeding El Niño years due to warm temperatures over the Bay of Bengal and the Arabian Sea (Naveena et al. 2021). Studies show that ENSO SST variability will be enhanced under the plausible emission scenario of Coupled Model Intercomparison Project-6 (CMIP6) emission scenarios (Cai et al. 2022). Recent years have witnessed very severe heat waves during the summers of 1998, 2003, 2005, 2015, and 2016 and with huge impacts on society (Neethu et al. 2020; Ghatak et al. 2017; Jenamani and Jendrakumar 2012). Heat waves will be more intense, more frequent, and long lasting in the future (Meehl and Tebaldi 2004). Increasing surface air temperature will significantly increase heat-related mortality and morbidity. During 1978-2014, heat waves caused 12,273 fatalities in India (Malik et al. 2021), and recent years have witnessed very severe heat waves with more than 2500 lives lost in 2015 (Dube et al. 2021; Pattanaik et al. 2017). The consecutive day and night heat waves are projected to increase, which has severe implications for public health and increases heat-related mortality in India (Mukherjee and Mishra 2018). The major population of India depends on agriculture for their livelihood and the agricultural system has to provide food for 17.5% of the world's population from 2.4% land and 4% water resources (Rao et al. 2016). Currently, more than 1.25 billion people in India are involved in outdoor activities (Panda et al. 2017). Studies show that by the end of the 21<sup>st</sup> century, the intensity of heat waves will be extreme in the densely populated agricultural regions of the Ganges and river basins (Im et al. 2017). At the end of this century, due to heat stress, work performance will decrease 30- 40% (Koteswara Rao et al. 2020).

Current studies of the CMIP6 heat wave projections over India are limited to the magnitude index of the heat wave (Das and Umamahesh 2022) and the characteristics of the heat wave in three cities in South India (Nandi and Swain 2022). There is a wide regional variation in temperature in India, as it extends from the tropics to the subtropics, as well as various landscape features of complex terrains such as plains, coastal lines, and mountains. Regional quantification of projected heat wave characteristics from CMIP6 climate models under plausible scenarios is lacking in the Indian region. In this study, we explore the regional analysis of historical and projected changes in the characteristics of heat waves in the seven temperature homogeneous zones (THZ) of India. Studies on projections are mostly done with a multi-model ensemble where the models have equal weighting even though wide dispersion exists among climate models. Hence, it is necessary to identify good skill models over each study region to improve the reliability of HW projections. The reliability assessment of the CMIP6 models is performed based on the distribution of the linear trend in the daily maximum temperature ( $T_{\max}$ ) and the correlation of seasonal  $T_{\max}$  with Niño 3.4 indexes at each THZ for the historical period. The four climate change scenarios SSP126, SSP245, SSP370, and SSP585 of CMIP6, based on Shared Socioeconomic Pathways (SSPs) are used. The present study focused on projected spatiotemporal changes in heat wave characteristics over THZ such as the number of heat wave days, the number of HW events, intensity, and the area of occurrence of HW days. Here, we will address a) how the HW characteristics change under different climate change scenarios, whether varying or uniform change, b) how it varies in different THZ, and c) the identification of zones of India which are going to be more vulnerable in the future.

## 2 Data and methodology

### 2.1 Study area and data

Based on the spatio-temporal distribution of surface air temperature, India is classified (<https://www.tropmet.res.in/>) into seven temperature homogeneous zones (THZ) (Dash and Mangain 2011; Purnadurga et al. 2017; Kumar and Sarthi 2019; Madhu et al. 2015; Chakraborty et al. 2017). Zones are North West (NW), North Central (NC), West Coast (WC), East Coast (EC), Interior Peninsula (IP), Western Himalaya (WH) and North East (NE) (Fig. 1a). Here we have used the high-resolution daily gridded  $T_{\max}$  ( $1^\circ \times 1^\circ$ ) data developed by the India Meteorological Department (IMD) for the period of 1951–2014 (Srivastava et al. 2009). Here Niño 3.4 indexes is used for estimating the correlation of El Niño with  $T_{\max}$ , which is the 3-month running average SST anomalies over  $5^\circ\text{S}$ – $5^\circ\text{N}$ ,  $120^\circ\text{W}$ – $170^\circ\text{W}$  and the data is generated using ERSST.v5 ([https://www-origin.cpc.ncep.noaa.gov/products/analysismonitoring/ensostuff/ONI\\_v5.php](https://www-origin.cpc.ncep.noaa.gov/products/analysismonitoring/ensostuff/ONI_v5.php)).

The bias-corrected gridded daily maximum temperature data have been developed by Mishra et al. (2020) for the South Asian regions [https://zenodo.org/record/3987736#.Yp\\_kp\\_nhVH5](https://zenodo.org/record/3987736#.Yp_kp_nhVH5) and red this data is used in many studies on heat waves and cold waves (Shetty et al. 2023; Bhattacharya et al. 2023; Kumar et al. 2023; Rao et al. 2023). Empirical Quantile Mapping is used for the bias correction of the data and the observational data of reference is IMD gridded  $T_{\max}$  data. The 13 CMIP6 models (Table S1) of various resolution of daily  $T_{\max}$  has statistically downscaled and bias-corrected to a resolution of  $0.25^\circ \times 0.25^\circ$ , for the months of April to June are used in the study. The  $T_{\max}$  for historical (1951–2014) and

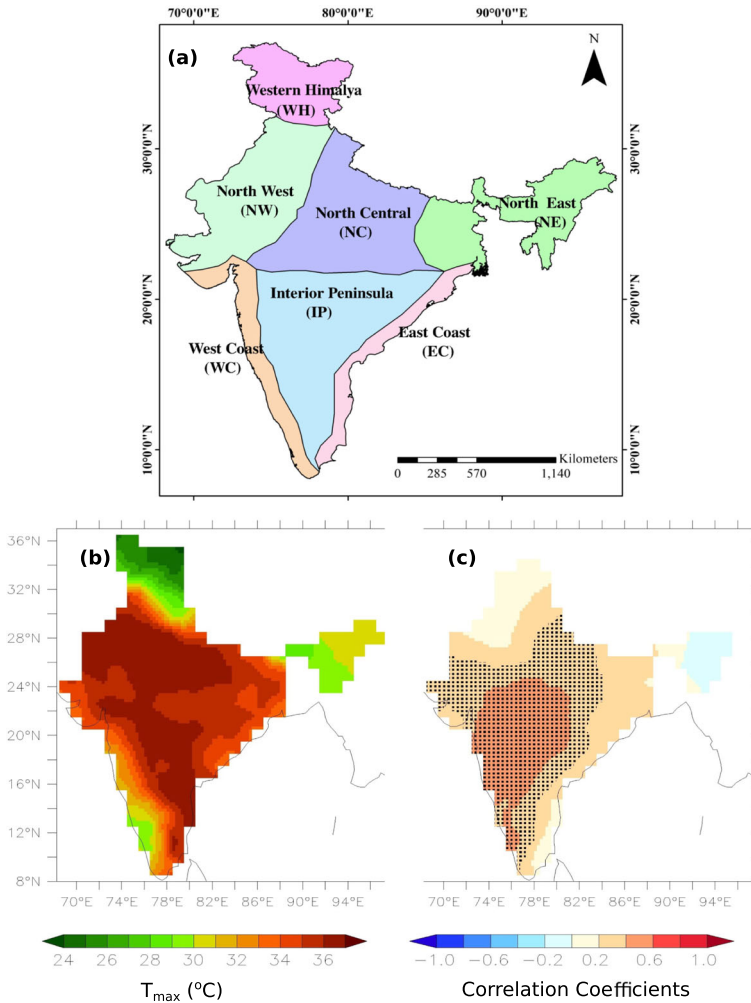


**Fig. 1** (a) Seven temperature homogeneous zones of India, (b) The seasonal mean of maximum temperature ( $^{\circ}\text{C}$ ) for 1951-2014 during April-May-June from IMD gridded data, (c) Lag correlation of observed mean AMJ maximum temperature with DJF Niño 3.4 indexes. The correlation that is significant at a confidence level 95% is highlighted with black dots

projections (2015-2100) under plausible scenarios SSP126, SSP245, SSP370, and SSP585 are used here. Where SSP126 is a mitigation scenario that suggests that by the end of the 21<sup>st</sup> century, the radiative forcing will be 2.6  $\text{Watt}/\text{m}^2$ , which is low forcing that combines low vulnerability with low challenges. SSP245 is a medium range of future forcing pathways with a radiative forcing of 4.5  $\text{Watt}/\text{m}^2$  by 2100. SSP370 is a baseline scenario with medium-to high-range future forcing with radiative forcing 7  $\text{Watt}/\text{m}^2$  by 2100 and fills the gaps in the CMIP5 forcing pathways. SSP585 is an emission scenario with an emission high enough to produce 8.5  $\text{Watt}/\text{m}^2$  radiative forcing by the end of this century (Eyring et al. 2016). To find the correlation of maximum temperature and Niño 3.4 indexes, we used the 13 CMIP6 models SST monthly data for the historical (1951-2014) period retrieved from the Earth

System Grid Federation, <https://esgf-node.ipsl.upmc.fr/search/cmip6-ipsl>. All data sets are bilinearly interpolated into a 0.25° X 0.25° common grid.

## 2.2 Methodology

There is no unanimous definition for HW and mostly region-based, but 90<sup>th</sup> percentile of threshold is widely used for the identification of heat waves globally as well over India (Perkins et al. 2012; Rohini et al. 2016; Panda et al. 2017; Perkins-Kirkpatrick and Lewis 2020; Das and Umamahesh 2022; Dubey et al. 2021; Russo et al. 2014). The 90<sup>th</sup> percentile threshold of  $T_{max}$  in THZ are NW (40.86°C), NC (41.51°C), IP (39.54°C), WC (35.72°C), EC (38.44°C), WH (31.12°C), NE (36.04°C) which is in agreement with the IMD heat wave threshold of  $T_{max}$  for plains (40°C), coastal (37°C), and hilly region (30°C). The minimum number of consecutive hot days needed to declare a heat wave varies from region to region. The reason for opting for percentile thresholds is that the frequency of days that exceed these thresholds is evenly spread across space and has significance in all regions (Zhang et al. 2011). Also, the IMD heat wave definition is for the station observations, and this definition may not fully account for regional variations in temperature patterns across different parts of zones. In the present study, heat waves are identified when  $T_{max}$  exceeds the 90<sup>th</sup> percentile threshold on calendar days of  $T_{max}$  for at least three consecutive days. The 90<sup>th</sup> percentile threshold of  $T_{max}$  is based on the 5-day moving window, which is comparable to location and time of year. The period considered for the percentile threshold is 1951-2014. Linear regression has been used for the estimation of a linear trend and the Student’s t test for the significance test. The confidence level 95% with  $p < 0.05$  is considered significant. Here, Pearson’s correlation coefficient is used.

It is important to identify suitable models for each region rather than a simple ensemble, since model simulations have a large bias (Ramesh and Goswami 2014). The selection of a reliable model for each THZ is based on the historical performance of the CMIP6 model on the trend distribution in  $T_{max}$  and the relationship of  $T_{max}$  with large-scale climate variability such as ENSO on each THZ. One of the primary indicator of the reliability of future climate projections is the ability to accurately simulate observed trends (Ramesh and Goswami 2014). The criteria used for the selection of reliable models are

1. Linear trends in the seasonal mean of  $T_{max}$  of individual historical CMIP6 models compared with the observations over each THZ. Observations showing a significant increase (decrease) in the linear trend of  $T_{max}$  and those historical models showing a significant increase (decrease) in the linear trend are considered. If the observations show an insignificant increase (decrease) in the linear trend and the models follow the trend pattern of the observations is also considered (Table 1).

**Table 1** The selection criteria for identifying the reliable models

Observations linear trend / correlation	CMIP6 historical models linear trend/correlation			
	Significant positive	Significant negative	Positive	Negative
Negative	×	×	×	✓
Positive	×	×	✓	×
Significant negative	×	✓	×	×
Significant positive	✓	×	×	×

- The Pearson correlation coefficient is identified between the seasonal mean (AMJ) of  $T_{max}$  and the preceding season (December-February, DJF) Niño 3.4 indexes is identified. If the observations show a significantly positive (negative) correlation and the CMIP6 historical model shows a significantly positive (negative) correlation, they are considered. Similarly, models in agreement with observations in terms of insignificant positive or negative correlation are also considered (Ramesh and Goswami 2014) (Table 1).

The simulations of the CMIP6 historical model that meet both criteria (Table 1) are selected as reliable models for each THZ (Table 2). We considered that the model performed well in historical periods and is assumed to be reliable in the future. We have investigated the historical and projected changes in  $T_{max}$  distribution, and the heat wave characteristics in each THZ with the mean of the selected reliable CMIP6 models of the respective regions. The characteristics addressed are

- Number of heat wave days
- Number of heat wave events
- Heat wave intensity
- Area coverage of heat waves

Days in which  $T_{max}$  is above the 90<sup>th</sup> percentile threshold of  $T_{max}$  are considered warm days, and if the condition persists for three or more days, it is a heat wave. The total number of days in a season that satisfy the HW criteria are the HW days. The total number of heat waves in the season is called heat wave events. The intensity is the average magnitude ( $T_{max}$ ) of the heat waves. The total areas experienced by heat waves in a year are expressed as the area coverage of heat waves. The projected change in the heat wave characteristics is calculated as the difference in the projected mean from the historical mean. The projected change in the coverage area is quantified by normalizing the projected change with respect to the historical mean, expressed as a ratio.

$$Projected\ change = \frac{Mean_{projection} - Mean_{historical}}{Mean_{historical}}$$

**Table 2** List of reliable models, where ✓ show the selected models over each zones

Models	NW	NC	WC	EC	IP	WH	NE
ACCESS-CM2	×	×	✓	×	×	×	×
ACCESS-ESM1-5	×	×	✓	×	×	×	×
BCC-CSM2-MR	×	×	×	×	✓	×	×
CanESM5	×	×	✓	×	×	×	×
EC-Earth3	×	×	✓	×	✓	×	×
EC-Earth3-Veg	✓	✓	×	×	✓	✓	×
INM-CM4-8	×	×	×	✓	✓	✓	×
INM-CM5-0	×	×	×	×	✓	×	×
MPI-ESM1-2-HR	×	✓	✓	×	✓	×	×
MPI-ESM1-2-LR	✓	✓	×	×	×	×	✓
MRI-ESM 2-0	×	×	×	×	×	×	×
NorESM2-LM	×	×	×	×	✓	×	✓
NorESM2-MM	×	×	×	×	✓	×	×

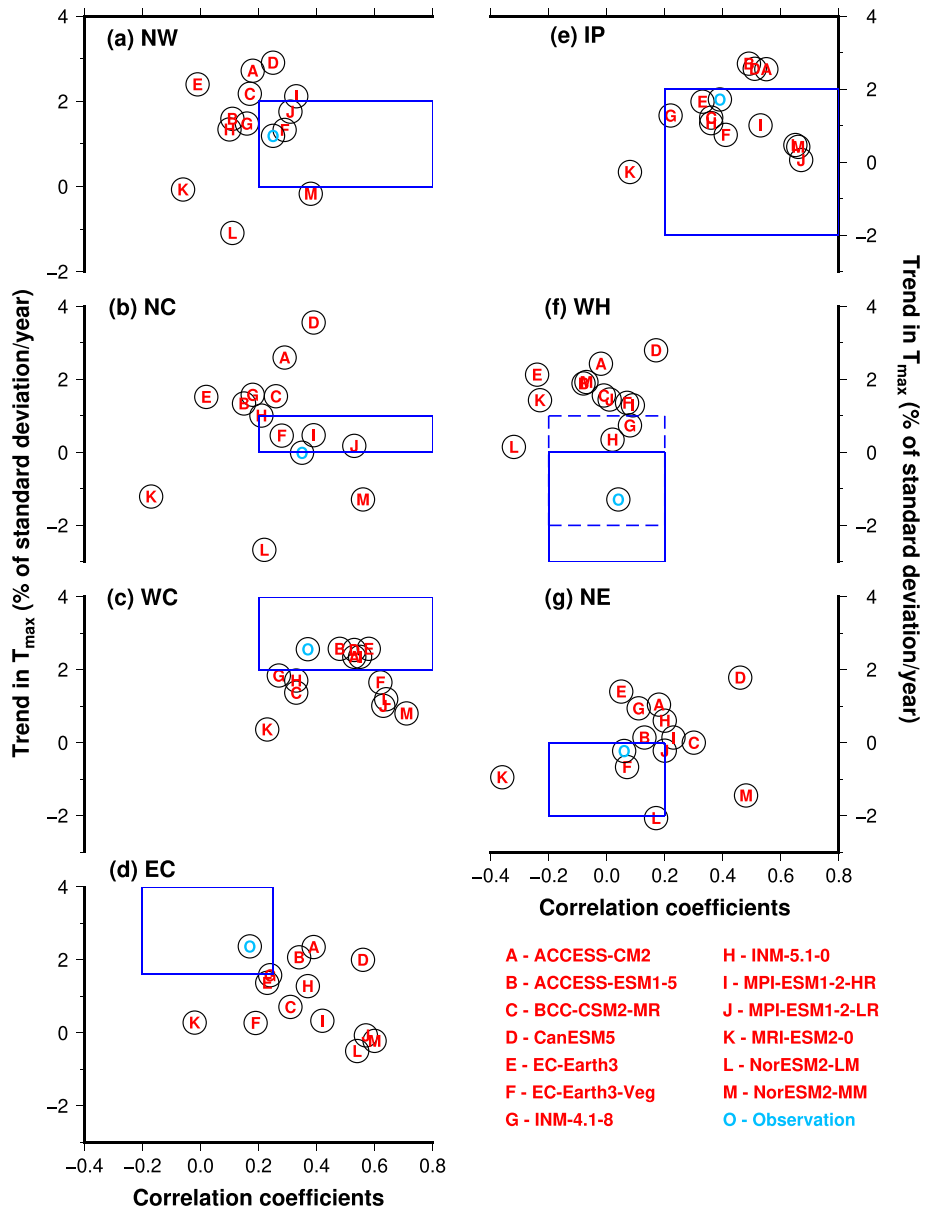


**Fig. 2** Selection of a reliable CMIP6 model for each temperature homogeneous zones based on the seasonal mean trend of  $T_{max}$  normalized with the standard deviation (%) and the lag correlation of the seasonal (AMJ)  $T_{max}$  with the seasonal (DJF) Niño 3.4 indexes. Models within the blue box are selected as reliable models for each region. For WH, selected models are inside the dotted box

## 3 Results

### 3.1 Selection of reliable models

The selection of reliable models for each THZ is based on the performance of models in two statistical quantities like the trend in the seasonal mean of  $T_{\max}$  and correlation between the AMJ seasonal mean  $T_{\max}$  over the Indian subcontinent with the preceding season DJF Niño 3.4 (Fig. 2). Extreme temperatures over the Indian subcontinent are related to ENSO, post-El Niño, the westerlies strengthen over the Indian subcontinent, leading to severe heat waves over most parts of India except NE (Naveena et al. 2021; Joshi et al. 2020). Figure 1c shows that the DJF mean of Niño 3.4 index has a strong correlation with the succeeding seasonal AMJ mean of  $T_{\max}$  in most of the THZ except NE. Models that are able to show the observed characteristics in both criteria are selected as the reliable model for the respective region (Table 2).

The observed trend in  $T_{\max}$  is significantly increasing in EC, the ACCESS-CM2, ACCESS-ESM1-5, CanESM5 and INM-CM4-8 models exhibit a significantly increasing trend.  $T_{\max}$ -Niño 3.4 index correlation is insignificant positive over EC and the models EC-Earth3, EC-Earth3-Veg, INM-CM4-8 have an insignificantly positive correlation. INM-CM4-8 is the only model that is in agreement with the observations in both the selection criteria and is selected as the reliable model for EC (Fig. 2d). Observations show significant positive  $T_{\max}$ -Niño 3.4 index correlation over WC (Fig. 1c) and all the models exhibit correlation features in the region. Although the observations show a significant increase in the trend of  $T_{\max}$  ( $p < 0.05$ ), the models that agree with the trend of observations are ACCESS-CM2, ACCESS-ESM1-5, CanESM5, EC-Earth3 and MPI-ESM1-2-HR (Table 2). Over NW and NC observations show a significant positive correlation and an insignificant positive trend in  $T_{\max}$  (Fig. 2a and b). The selected models are reliable in representing the observed features; over NW are EC-Earth3-Veg and MPI-ESM1-2-LR whereas over NC, EC-Earth3-Veg, MPI-ESM1-2-HR, and MPI-ESM1-2-LR.  $T_{\max}$  over IP has a strong positive correlation with Niño 3.4 indexes and all models can simulate the significant positive correlation except MRI-ESM 2-0. The trend in  $T_{\max}$  is significantly increasing over IP, the historical models BCC-CSM2-MR, EC-Earth3, EC-Earth3-Veg, INM-CM4-8, INM-CM5-0, MPI-ESM1-2-HR, NorESM2-LM, and NorESM2-MM are able to perform both criteria and therefore are considered reliable models of IP. Over NE, the observations exhibit an insignificant decreasing trend in  $T_{\max}$ , the models that indicate the observed trend are EC-Earth3-Veg, MPI-ESM1-2-LR, MRI-ESM 2-0, NorESM2-LM, and NorESM2-MM. Whereas the  $T_{\max}$ -Niño 3.4 index correlation over NE is insignificant positive, the models CanESM5, EC-Earth3-Veg, INM-CM4-8, INM-CM5-0 and MPI-ESM1-2-HR show an insignificant positive correlation (Fig. 2g). Therefore, EC-Earth3-Veg, MPI-ESM1-2-LR, and NorESM2-LM are reliable in simulating both criteria and are the selected models for NE. Observations show an insignificant negative trend in WH, but none of the models exhibits the observed features. This may be due to the challenge faced by climate models on complex terrains or less dense observation stations on the WH (Shah and Mishra 2014; Mishra et al. 2020). Therefore, in WH, we have slightly modified selection criteria and models that show an insignificant trend are considered, such as INM-CM4-8 and INM-CM5-0 (Fig. 2f). Although the correlation is insignificantly positive and six models show an insignificantly positive correlation, among these, INM-CM4-8 and INM-CM5-0 perform well in both features. MRI-ESM 2-0 cannot simulate the observed features in the  $T_{\max}$  trend and correlation of  $T_{\max}$  simultaneously, and therefore it is not a suitable model for any of the regions (Table 2).



### 3.2 Distribution of daily maximum temperature

In India,  $T_{\max}$  has a large spatial variability during AMJ, the seasonal mean of  $T_{\max}$  over NW (37.95°C), NC (38.5°C), and IP (37.2°C) is high during AMJ, and the coastal zones are warm WC (33.94°C) and EC (36.26°C). The western part of NE is warm compared to the other regions and the mean  $T_{\max}$  is 33.09°C, while the major parts of WH have a relatively low  $T_{\max}$  and the seasonal mean is 27.48°C (Fig. 1b).

#### 3.2.1 Daily maximum temperature anomaly distribution

During 1951-2014, observations show  $T_{\max}$  anomaly over most of the regions is increasing, over WC, EC, and IP it is significant (95% confidence level) and insignificant over WH and NW, while over NC and NE it is an insignificant negative trend (Table 3). Linear trends of the model during the same period show significant changes in most of the THZ except WH. The average  $T_{\max}$  anomaly distribution of selected CMIP6 models is in good agreement with the observations (Fig. 3). Future projections of the anomaly of  $T_{\max}$  of the CMIP6 models show a significant increase trend ( $p < 0.05$ ) in different SSP scenarios, except over WC in SSP126 (Table 3). The highest rate of an increasing trend in  $T_{\max}$  is over WC (0.51°C/decade), followed by NW (0.41°C/decade) under SSP585. At the end of the 21<sup>st</sup> century, the  $T_{\max}$  anomaly is likely to be highest over WC (>4°C) under SSP585 and least over NE (2.5°C). The seasonal anomaly of all model composite is overestimated compared to the mean of the selected model in most zones except WC (Fig. 3). By 2100 the  $T_{\max}$  anomaly is likely to be maximum under the high emission scenario (SSP585) and least in the mitigation scenario (SSP126), of the order SSP585 > SSP370 > SSP245 > SSP126. The highest seasonal maximum  $T_{\max}$  anomaly is likely to be in NW, WH, EC, and in small pockets in NE with more than 5°C under the scenarios SSP370 and SSP585 and greater than 4°C under the scenarios SSP126 and SSP245. Over WC, parts of IP, and southeastern parts of NE have recorded comparatively low  $T_{\max}$  anomaly, less than 2°C under SSP126 and in the range of 2.5-3.5°C under SSP585 (Fig. S1).

#### 3.2.2 Area coverage of maximum temperature

Here we estimate the historical and projected changes in the distribution of  $T_{\max}$  compared to the mean of selected models and all models composite. The seasonal mean of  $T_{\max}$  in NW,

**Table 3** The linear trends (°C/decade) in seasonal average  $T_{\max}$  anomaly for the historical and projections from selected model mean over each THZ

Zones	Obs	Hist	SSP126	SSP245	SSP370	SSP585
NW	0.09 <sup>x</sup>	0.12	0.11	0.24	0.34	0.41
NC	-0.001 <sup>x</sup>	-0.16	0.10	0.21	0.29	0.35
WC	0.12	0.13	0.12	0.25	0.41	0.51
EC	0.13	0.10	0.002 <sup>x</sup>	0.13	0.21	0.33
IP	0.11	0.07	0.06	0.17	0.27	0.36
WH	0.02 <sup>x</sup>	0.04 <sup>x</sup>	0.05	0.15	0.29	0.37
NE	-0.007 <sup>x</sup>	-0.06	0.06	0.18	0.26	0.36

<sup>x</sup> denotes the trends that are NOT statistically significant at the 95% level

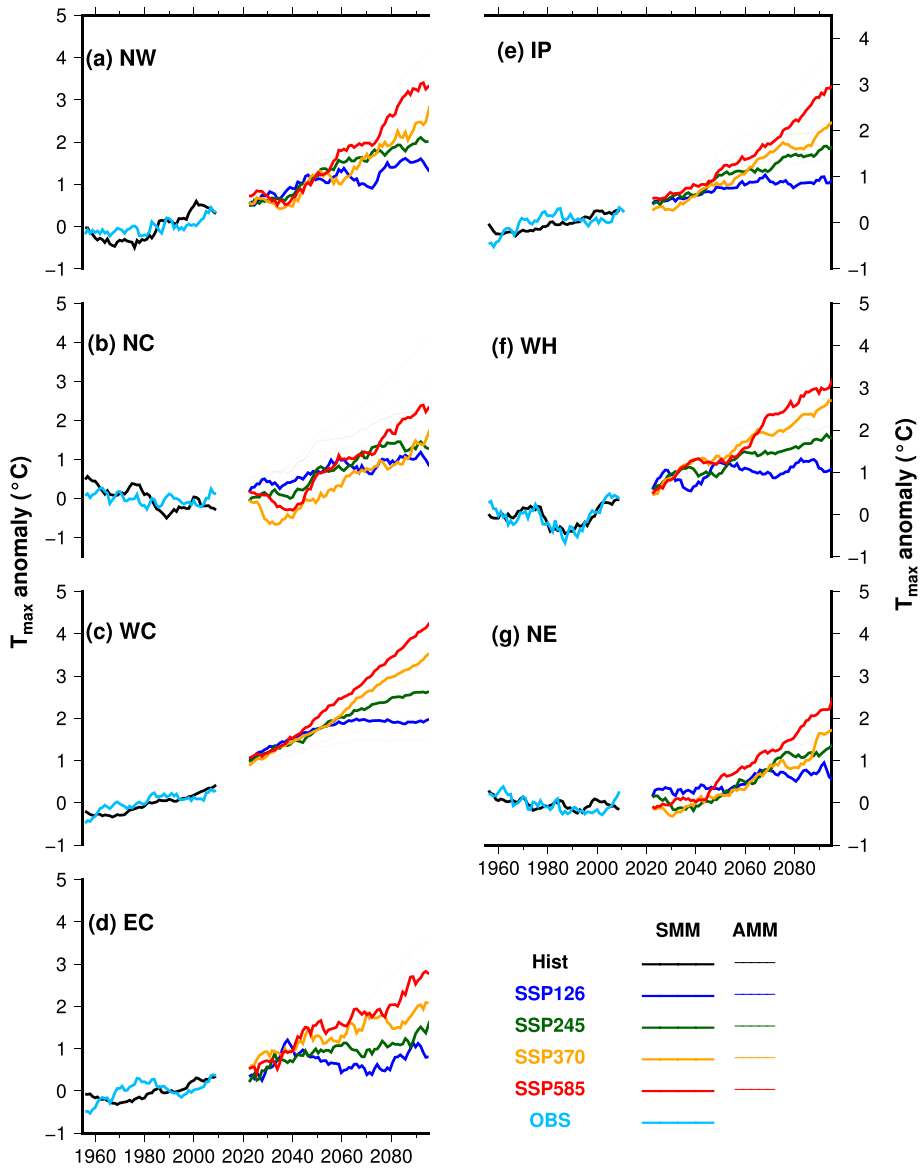


**Fig. 3** Time series of daily  $T_{max}$  anomalies (°C) from the Selected Models Mean (SMM) and All Models Mean (AMM) for the historical and projected scenarios with 11-year smoothing

NC, IP, CE, and most parts of WC are below  $40^{\circ}\text{C}$ , in WH and NE is  $30^{\circ}\text{C}$  (Fig. 1b). Also, the area coverage of the maximum temperature of THZ under different categories shows that in zones like NW, NC, WC, EC, and IP, the maximum area of coverage is in the range of  $37\text{--}40^{\circ}\text{C}$ , while WH and NE are in the range of  $27\text{--}30^{\circ}\text{C}$  and  $30\text{--}33^{\circ}\text{C}$  (Fig. 4). Therefore, to identify the trend in the distribution of areas of occurrence of higher maximum temperatures in zones, we used the thresholds of  $40^{\circ}\text{C}$  for NW, NC, WC, EC, and IP, and  $30^{\circ}\text{C}$  for WH and NE. Additionally this threshold of each zone is close to the 90<sup>th</sup> percentile threshold of

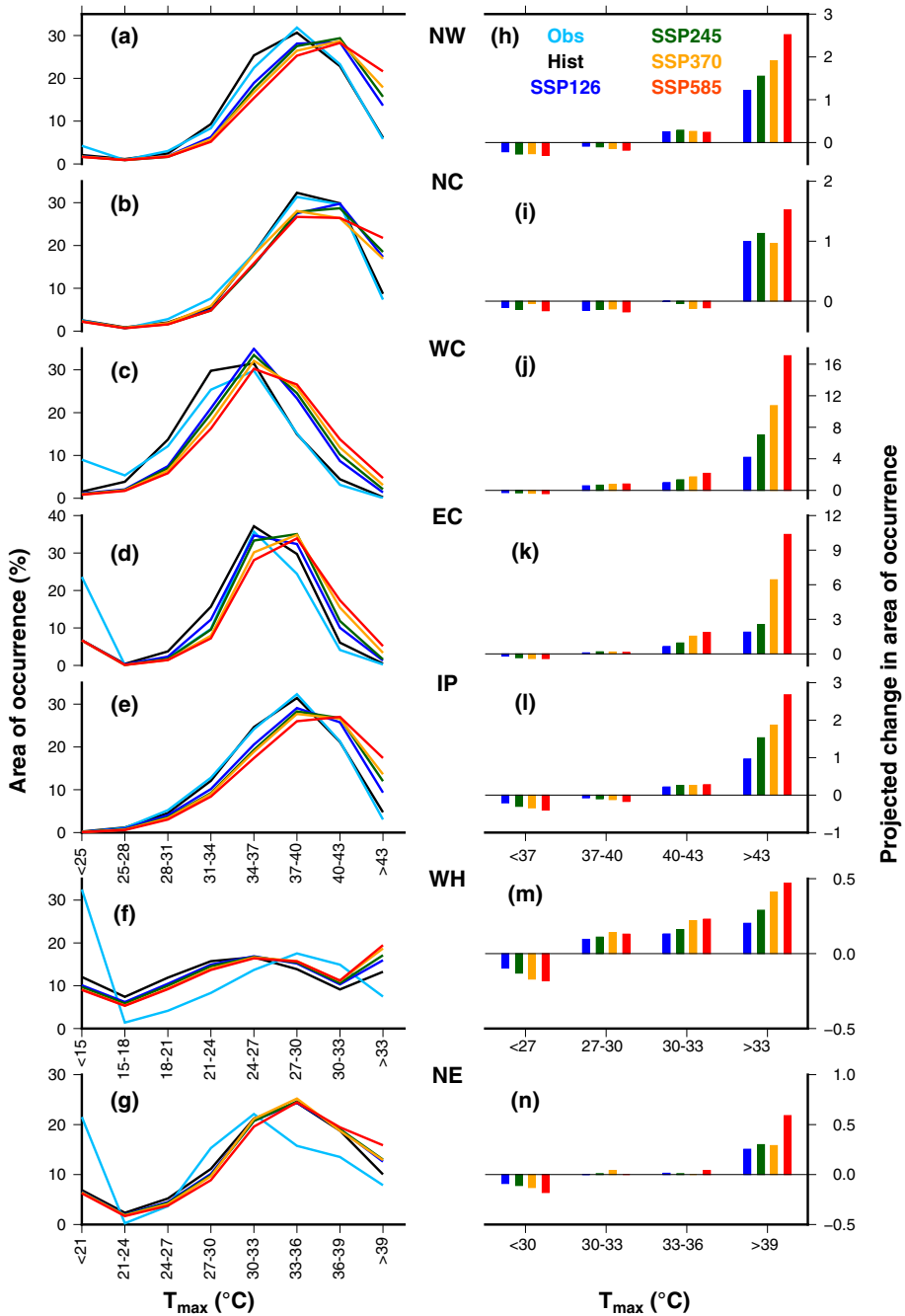


**Fig. 4** Fig. (a-g) is the distribution of area of occurrence (%) for each  $T_{max}$  (°C) category and Fig. (h-n) is the ratio of projected change in area w.r.t historical for the extreme categories of  $T_{max}$  (°C) over all the seven THZ from the selected model mean of various SSP scenarios, historical period of CMIP6 (black), and OBS (blue)

$T_{\max}$ . The observations and the trend of the models in the area of occurrence of  $T_{\max}$  above the threshold temperature of the respective region are illustrated in Fig. S2. Observations of EC, IP, WH, and NE show a significant increase in the area of occurrence above the threshold, whereas the all models mean are overestimated since there is a wide dispersion between the CMIP6 model. The observations show an insignificant increase in the area over NW, NC, and WC, but all model composites are overestimated. The trend in the area of occurrence of the selected model mean gives a better approximation than all models mean in NW, NC, EC, and IP in the range of 0.5–2.5 % of a standard deviation per year, except for WC, where the mean of the selected model is overestimated. Over WH, the trend in the area of occurrence of the selected model mean is underestimated. There is variability in the distribution of the trend in the NE, where the observations show a positive trend and selected models exhibit a negative trend. The CanESM5 model shows a higher linear trend in the area of occurrence of extreme  $T_{\max}$  on all the THZ compared to other models. The projected  $T_{\max}$  above the threshold is widely spreading under different SSP scenarios, increasing from the mitigation scenario to the high emission scenario in the order SSP126, SSP245, SSP370 and SSP585. The area of occurrence is projected to increase over all zones.

The historical and projected area of occurrence in  $T_{\max}$  distribution from the selected model mean is shown in Fig. 4a–g. The projected changes in area of occurrence in  $T_{\max}$  extremes are shown as the ratio between the projected change (projected minus historical) and historical mean (Fig. 4h–n). For the NW, NC, WC, EC and IP zones (Fig. 4a–e) the base for the  $T_{\max}$  categorization is the same, and for the other two regions the seasonal mean of  $T_{\max}$  is comparatively lower and hence used the different categorization. During the historical climate, in NW and NC, 80% of the area has  $T_{\max}$  in the range of 34–43°C, where the highest (30%) is under 37–40°C category. The projections show that the areas of  $T_{\max} < 40^\circ\text{C}$  are decreasing and above that it is increasing in India. Under the SSP585 scenario, in NW and IP, the area of occurrence of  $T_{\max}$  greater than 43°C is likely to double by 2100 (Fig. 4h). In the case of NC, the regions with  $T_{\max}$  below 43°C are decreasing, above that it is increasing under four projected scenarios (Fig. 4i). The selected models show that 60% of the area over the WC is in the range of 31–37°C whereas 70% of the EC is under 34–40°C during 1951–2014. During the same period, the coastal zones with  $T_{\max}$  above 43°C have negligible area but by the end of this century this extreme category likely spread over the regions, with a 16-fold increase over WC and more than 10-fold increase over EC under SSP585. In WH and NE, there is uncertainty with the observations (Fig. 4f and g) as GCMs are unable to project reliable climate change information over complex topographies (Zhu et al. 2020). The ratio of projected changes in the area of occurrence of extreme categories of  $T_{\max}$  in WH and NE is less than in the other zones.

### 3.3 Projected changes in characteristics of heat waves

This section discusses the projected changes in the number of HW events, duration, HW intensity, and warm days in terms of spatio-temporal distribution under climate change scenarios, and are represented in the near future (2025–2050), future (2051–2075), and far future (2076–2100).

#### 3.3.1 Spatio-temporal distribution of heat wave days and events

The temporal distribution of HW days (Fig. 5) indicates the close approximation of the composite of selected models to the observations with a bias of  $\pm 1$  day over most of the

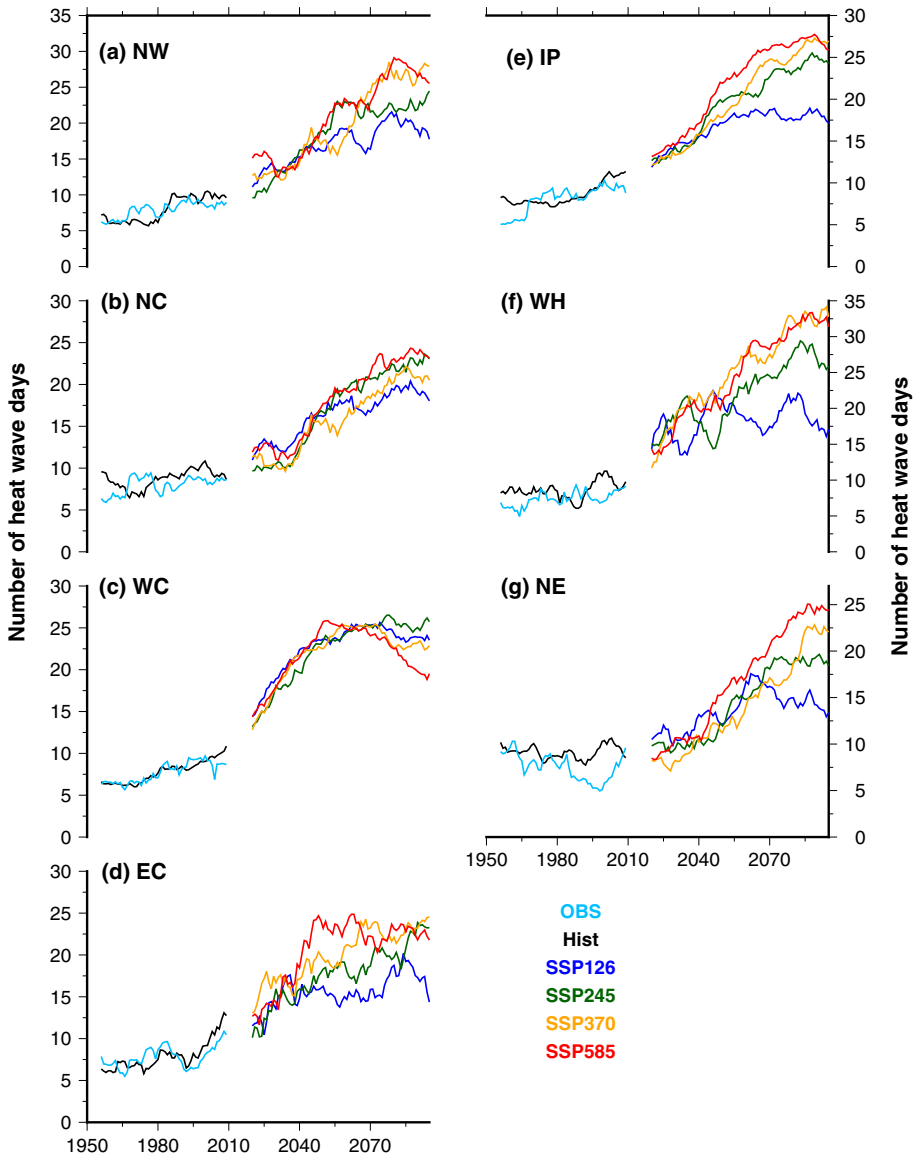


**Fig. 5** Distribution of heat wave days (days/year) from OBS and the selected models means of historical, projections from multiple SSP scenarios over all the THZ with 11-year smoothing

THZ except for WH (2 days) during the historical period (1951-2014). Figure 5 shows a historical mean of 8-9 days of HW per season in most of THZ and is projected to increase by approximately 15 days over NW, NC, EC, and IP, while WC and WH by approximately 20 days per season in the near future. In the future, in most of the zones, the HW days under SSP126 are less than 20, while under SSP370 and SSP585 about 20-25 except for NE (15-18 days). In the far future, most of the zones are projected to have more than 25 days of HW per season, except WC (Fig. 5). In the same period, the mean HW days change from the

**Table 4** The projected increase in heat wave days averaged under different scenarios over each THZ

Zones	Near future	Future	Far future
NW	6.94	12.56	16.13
NC	4.32	9.50	12.61
WC	12.42	16.70	15.18
EC	8.62	11.49	12.97
IP	7.20	12.72	14.78
WH	10.37	15.45	19.21
NE	1.75	6.92	10.35
All India	7.37	12.19	14.46

historical base period, over NW (16.1 days), NC (12.6 days), WC (15), IP (14.7 days), WH (19.2 days), EC (12.9 days) and relatively less change over NE (10.35 days), while the mean of all India is 14.5 days (Table 4). In WC, the projected change shows minimal variation between all the climate change scenarios to the future, but wide variation in the far future (Fig. 5c).

The spatial distribution in HW days shows an increase over most of the zones except some parts of the NE in the near future (Fig. 6-I). In the same period, relatively less increase (1-4 days) is likely to occur over parts of NE, while, over parts of WH, NW, IP, NC and EC are likely to increase about 8-12 days. In the future, the highest increase in HW days (>16 days) is over WC, WH, parts of IP and NW under SSP370 and SSP585. In the far future, severe increase in HW days over WH (>20 days), NW (16-24 days), and IP (16-20 days) under SSP370 (Fig. 6 -I k). Figure 7a-c show that over WC, heat wave days are increasing until the future, expected a small decrease under SSP370 and SSP585 during the far future. The projected heat wave days show a significant increasing trend over most of the zones, the highest is to be over WH under SSP370 and SSP585 (>2.5 days/decade), where a relatively less trend is over the coastal zones (<1.5 days/decade) (Fig. 9a). NE has a relatively smaller number of HW days, but shows a significant increase in heat wave days, 2.4 days/decade under SSP585 (Fig. 9a).

Warm days are the total number of days in which  $T_{\max}$  is greater than the 90<sup>th</sup> percentile threshold (including HW days). During the historical period, most zones have 9.5-10 warm days per season, while HW days are about 8-9 days. Over WC, warm days are likely to increase about 50% days of the season (Fig. 8). In the future period (2015-2100), WC is likely to have the highest number of warm days (Table 5), i.e. 37 days (SSP126), 42 days (SSP245), 47.4 days (SSP370), 52.14 (SSP585). This indicates that by the end of the 21<sup>st</sup> century the HW days (consecutive warm days) are decreasing in WC but the total number of warm days is increasing five-fold. Although a severe increase in HW days is projected in NW (1.6 times) and WH (1.9 times), the highest number of warm days of the season is likely to be in peninsular India (WC, EC, and IP), and the eastern part of WH under SSP370 and SSP585 (Fig. 8c and d). The increase in warm days over NE is approximately 2.4 times, but over NW, EC, IP and WH 3.7 times under SSP585 (Table 5), while the increase in HW days over these zones is approximately 1.5-2 times.

The spatial distribution in projections of HW events shows an increase over most of the zones of India except over some parts of NE during 2025-2050 (Fig. 6-II a to d). In the near future, the increase in HW events averaged in zones WC (1.7-1.9), EC (1.0-1.4), and WH

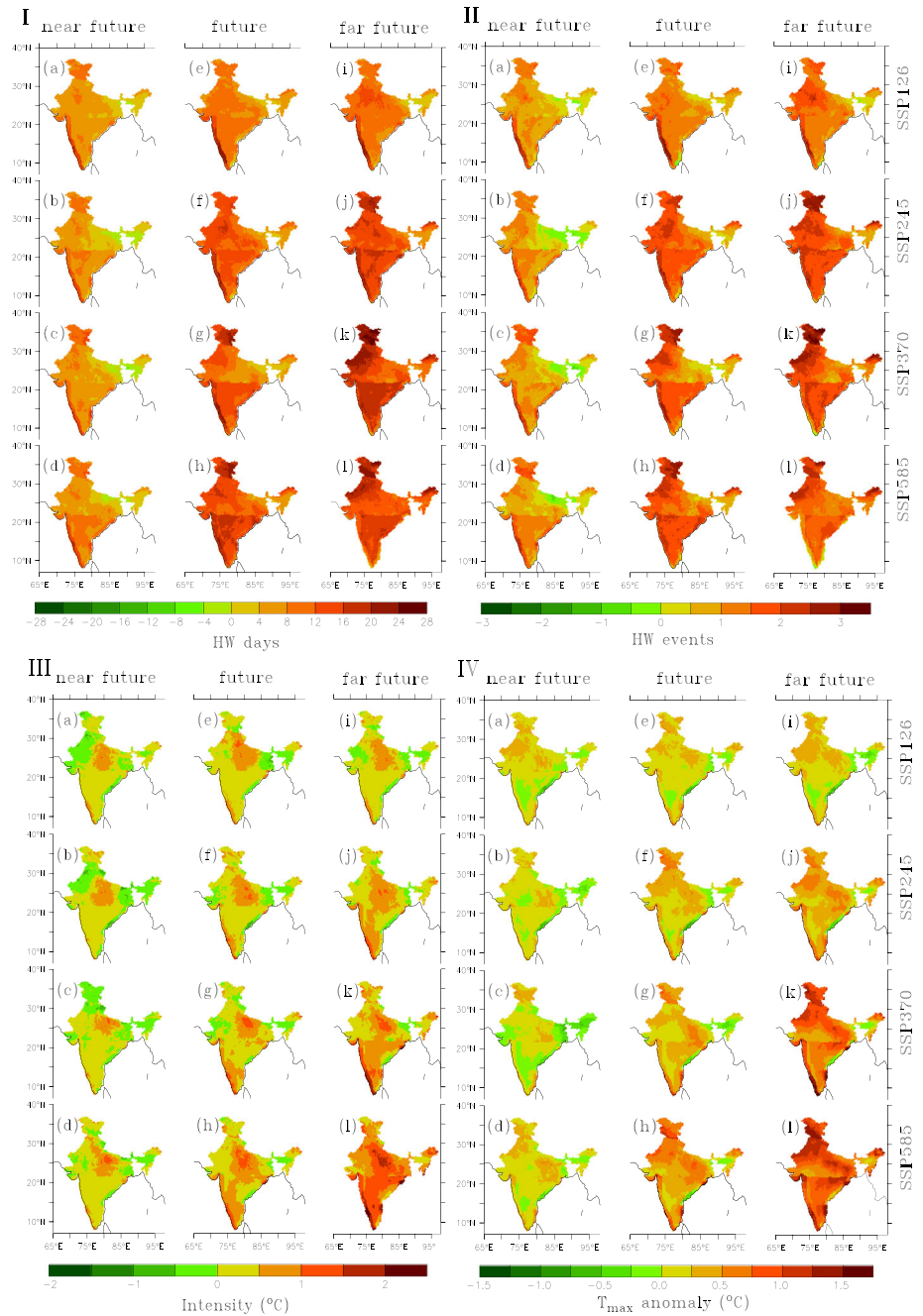


**Fig. 6** Projected change (SSP-historical) in the I) number of HW days II) HW events, III) intensity and IV)  $T_{max}$  anomaly during HW for the three periods near future (2025-2050), future (2051-2075), and far future (2076-2100) for multiple SSP scenarios. In each 1<sup>st</sup> row is SSP126, 2<sup>nd</sup> row is SSP245, 3<sup>rd</sup> row is SSP370, and 4<sup>th</sup> row is SSP585

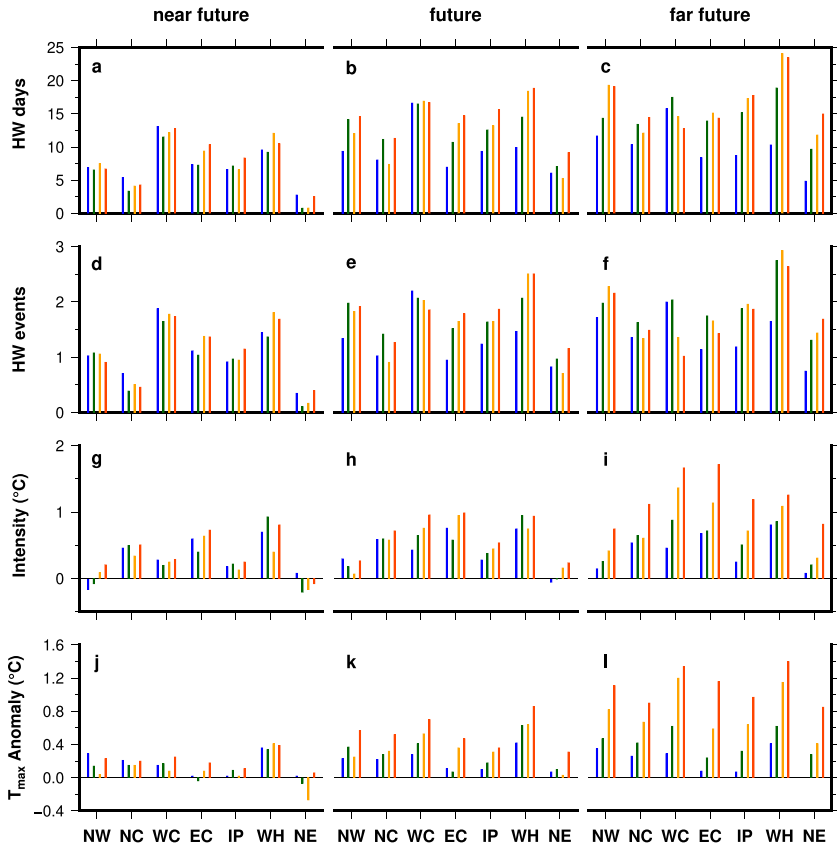


**Fig. 7** The projected changes in the heatwave characteristics averaged over each THZ for three periods. (a-c) the number of HW days, (d-f) the number of HW events, (g-i) HW days intensity, (j-l)  $T_{max}$  anomaly during HW days. The four scenarios are represented as SSP126-blue, SSP245-green, SSP370-yellow, SSP585-red

(1.4-1.8) is above the average of all India of 0.9-1.1 events. In the future, the increase in HW events is relatively less over NC and NE in the range of 0.5-1.5; the highest increase of more than 2 events is likely to be over eastern WH, central NW, and WC under SSP370 and SSP585. In the far future, more than 3 HW events are likely to increase over parts of NW and WH under SSP370 (Fig. 6-II k). The increase in events averaged over zones shows that WH (1.6-2.9 events), NW (1.7-2.3 events) are above the all-India average (1.4-1.9 events) and below are in the range of 1-2 events (IP and WC), 1.1-1.7 events (NC and EC), 0.7-1.7 events (NE) during the far future (Fig. 7d-f). The time series distribution of HW events shows that by the end of this century, NW and WH are likely to have 4.5 events in a season, and most of the other THZ is expected to have 3.5 events (Fig. S3h-n). Over WC, the number of events is declining to 2.5 events by the late future under SSP585 (Fig. S3j, Fig. 9b). The trend in HW events is less over coastal zones and the other zones are likely to have more than 0.15 events/decade. Among the climate change scenarios, SSP245 and SSP370 have the highest increasing trend in HW events in most of the zones. Insignificant increases in events are over EC and WH under SSP126 and also over WC under SSP370.



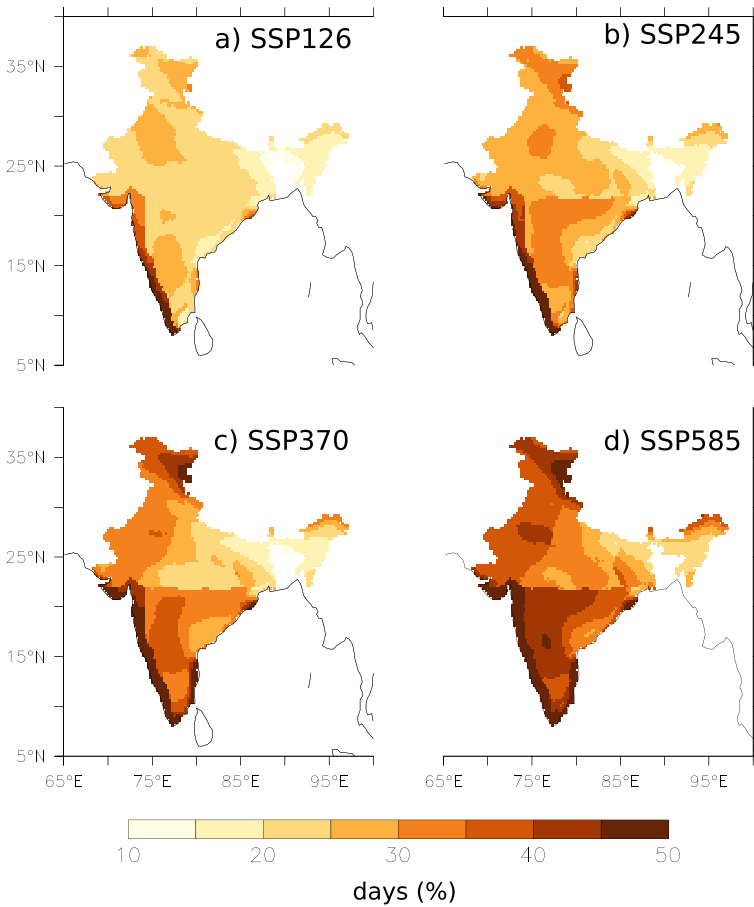


**Fig. 8** The projected warm days in the season AMJ (%) under scenarios SSP126, SSP245, SSP370, and SSP585

**Table 5** The average number of warm days during historical and projected scenarios over each THZ

Zones	Hist	SSP126	SSP245	SSP370	SSP585
NW	9.5	22.4	26	29.8	34.8
NC	10	21	23	22.3	28.1
WC	9.5	37	42	47.4	52.14
EC	10.2	20	24	32.3	36.54
IP	10	22	28	31	37
WH	10.2	23	28.1	36	37.7
NE	10	17	18.8	19.3	25

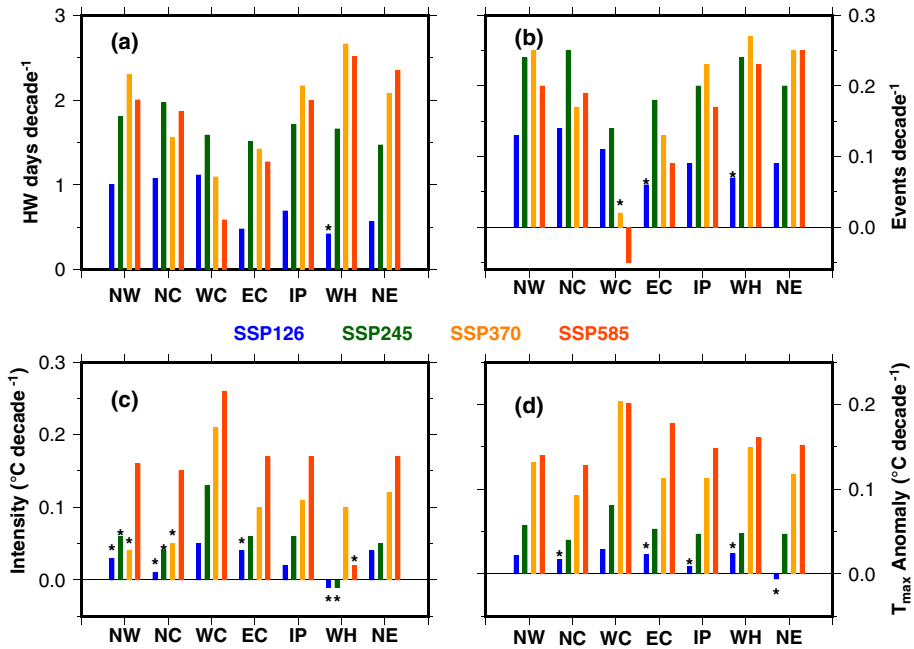


**Fig. 9** Projected linear trend in (a) number of heat wave days (b) heat wave events (c) heat waves intensity, and (d) heat wave days  $T_{max}$  anomaly ( $^{\circ}C$ ) from the projection scenarios SSP126, SSP245, SSP370 and SSP585 in each THZ. The linear trend which is NOT significant at 95% confidence level is marked as \*

### 3.3.2 Spatio-temporal distribution of heat waves intensity

The difference in the projected HW intensity from the historical HW intensity is discussed in this section. The spatial distribution of the projected change in heat wave intensity during the near future shows the highest increase ( $0.5-1.5^{\circ}C$ ) over NC, while decrease ( $0.1-0.5^{\circ}C$ ) over NW, NE, and parts of EC and WH (Fig. 6-III). In the future, highly intense zones with respect to the historical period are over NC and WC, an increase in HW intensity is about  $0.5-1.5^{\circ}C$  (Fig. 6-III e-h). In the far future, the intensity of HW in WC, IP, NC, and EC is likely to increase severely ( $>1^{\circ}C$ ) under SSP585, whereas intensity may decrease ( $0.1-0.5^{\circ}C$ ) in some regions of EC, NE, NW and WH under SSP126, SSP245, and SSP370. The projected change in heat wave intensity and HW days has a spatial variation, NC shows a significant increase in HW intensity, while the increase in HW days is least over there (Fig. 6I and III). The increase in intensity averaged over each THZ indicates that NC, WC, and WH have an intensity above the all-India average of  $0.24-0.39^{\circ}C$  during the near future. But in the future, the intensity of five zones (NC, WC, EC, IP and WH) will be well above the all-India average ( $0.44-0.53^{\circ}C$ ). During the far future, coastal zones are more vulnerable with an increase of  $1.7^{\circ}C$  under SSP585 whereas all India average is  $1.2^{\circ}C$  (Fig. 7g-i). The change in mean HW intensity from the recent decade to the last decade of the century is  $41.9^{\circ}C$  to  $43.25^{\circ}C$  (NC),  $40.8^{\circ}C$  to  $42.25^{\circ}C$  (NW),  $36.6^{\circ}C$  to  $38.5^{\circ}C$  (WC),  $39.5^{\circ}C$  to  $40.5^{\circ}C$  (EC),  $40.8^{\circ}C$  to  $42^{\circ}C$  (IP),  $36.4^{\circ}C$  to  $37.55^{\circ}C$  (NE) under SSP585 (Fig. S3a-g). The southern parts of WC, EC and NC are the densely populated regions of India, so an increase in the intensity of the HW will

adversely affect the large population and agriculture production of these regions. About 49% of the workers in India are employed in outdoor activities, and heat waves will severely affect them. The projections (2015–2100) show a significant increasing trend in intensity ( $p < 0.05$ ) over WC, IP, and NE (Fig. 9c). The present-day core heat wave regions are NW and NC, projected to have an insignificant increase in the intensity of HW under three scenarios, while SSP585 has a significant increase in intensity ( $0.15^\circ\text{C}/\text{decade}$ ). The projected trend in the intensity of HW in WC shows a significant increasing trend in the range of  $0.05^\circ\text{C}/\text{decade}$  (SSP126) and  $0.26^\circ\text{C}/\text{decade}$  (SSP585) (Fig. 9c), while trend in HW days more significant over WH (Fig. 9a). Hence there is a spatiotemporal variation in the distribution of HW days and HW intensity.

Projected change in  $T_{\text{max}}$  anomaly during heat waves shows a severe increase in NW, WC, WH and NC which are above all India average ( $0.1\text{--}0.2^\circ\text{C}$ ) and a decrease in the small areas of NE, EC and IP during 2025–2050 from the historical base period (Figs. 6-IV and 7j-l). In the future,  $T_{\text{max}}$  anomaly is widely increasing over most of the zones with more than  $0.5^\circ\text{C}$ , while the small regions of EC and NE have a decrease in the anomaly. In the far future, severe increases in anomaly ( $> 1^\circ\text{C}$ ) are projected over NW, WC, parts of NC, southern EC, and northern IP, while relatively small changes are projected over the northern side of EC and central NE under SSP370 and SSP585 (Fig. 6-IV k and l). In the far future, most of the zones will show an increase in the number of HW days and events but on the northern side of EC and central NE, there is a decrease ( $0.1\text{--}0.5^\circ\text{C}$ ) in intensity and  $T_{\text{max}}$  anomaly except under SSP585. The increase in  $T_{\text{max}}$  anomaly is  $0.3\text{--}1.3^\circ\text{C}$  over WC,  $0.1\text{--}1.2^\circ\text{C}$  over EC, and  $0.4\text{--}1.4^\circ\text{C}$  in WH under four climate change scenarios (Fig. 7l). The projected  $T_{\text{max}}$  anomaly distribution varies from the spatial distribution of intensity, some parts of IP are likely to have a decrease in the  $T_{\text{max}}$  anomaly, but the intensity of HW is increasing in the same regions, the change is about  $0\text{--}0.5^\circ\text{C}$  in the near future. The strength of the  $T_{\text{max}}$  anomaly is significantly increasing from the low emission scenario to the high emission scenario on the order of  $\text{SSP126} < \text{SSP245} < \text{SSP370} < \text{SSP585}$  (Fig. 7j-l, Fig. S3). In the mitigation scenario-SSP126, the projected trend in the  $T_{\text{max}}$  anomaly is insignificant over NC, EC, IP, and WH with less than  $0.03^\circ\text{C}$  per decade and a decreasing trend over NE (Fig. 9d). The highest trend in  $T_{\text{max}}$  anomaly is likely to be in the WC of  $0.2^\circ\text{C}$  per decade. In the last decade of this century,  $T_{\text{max}}$  anomaly will be maximum in the NW of  $5^\circ\text{C}$  under SSP585, followed by all other zones in the range of  $4\text{--}4.5^\circ\text{C}$ .

### 3.3.3 Area coverage of heat waves

This section describes the projected area of occurrence of different categories of heat waves. Heat waves are classified into four categories based on the duration of the HW, medium (3–5 days), long (6–8 days), severe (9–11 days) and extreme ( $> 11$  days). The ratio of projected change in the area of occurrence shows a 2 to 3 fold increase in areas of medium and long HW in all zones (Fig. 10), while severe and extreme heat waves are expected to extend in a wide area. The remarkable increase in the area of occurrence of the extreme category is likely to be over the WC of about 20-fold in all climate change scenarios (Fig. 10c). Under SSP585 the area of extreme categories increases about 12 times over IP and NW, and about 8 times over NC, EC, and WH, while under SSP370 it is 5-fold (NC), 10-fold (NW, EC, and IP) and 9-fold (WH). The area of severe heat waves increases to 4 to 6 times over all the zones where relatively widespread is over WC and WH. In NE, severe and extreme heat waves are projected to increase less than 2 times under SSP126 and SSP245, while extreme HW may increase to 4 times under SSP585.

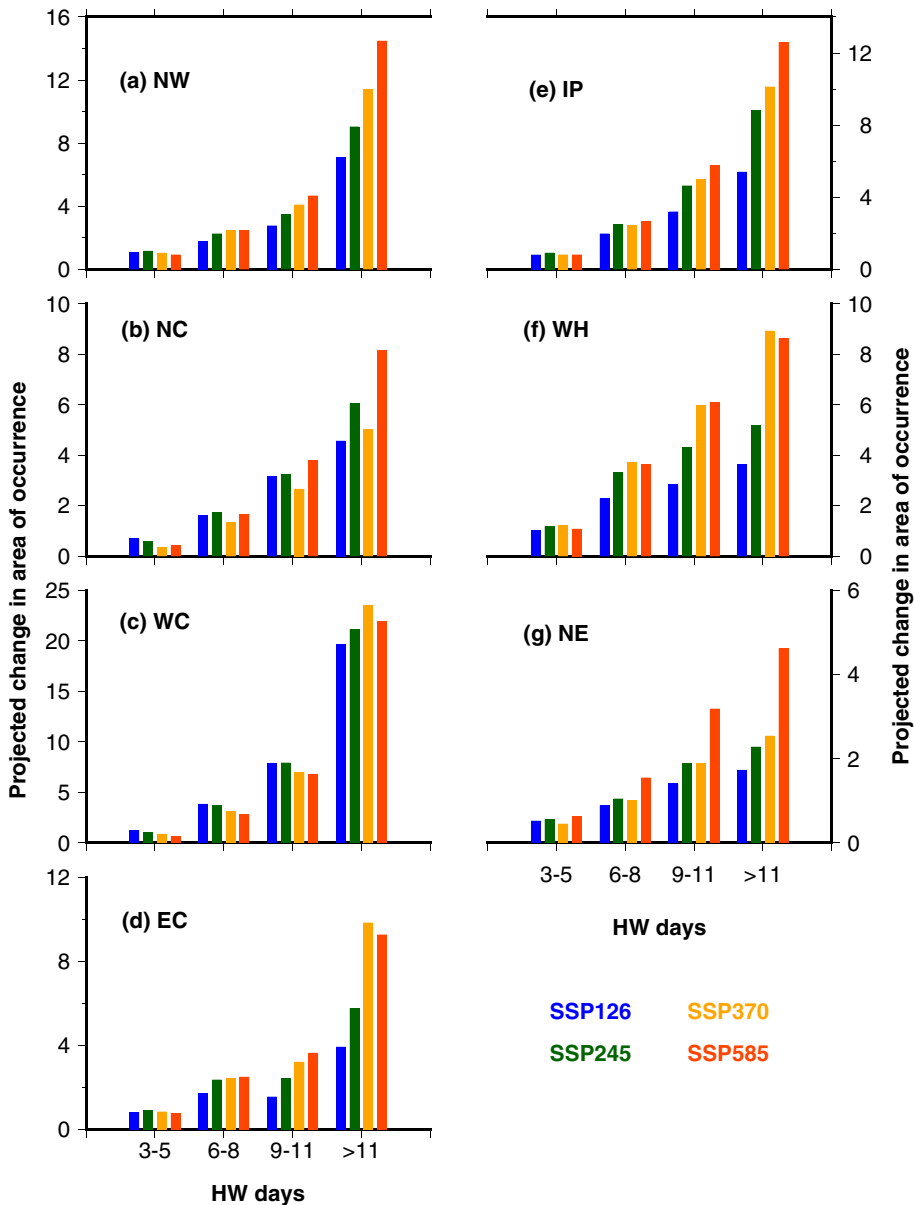


**Fig. 10** The ratio of projected changes in the area of occurrence for the different heat waves, based on the days of occurrence

Thus the projections from reliable CMIP6 models show that heat waves over each temperature homogeneous zones will become more frequent and intense with an exacerbating increase in the occurrence of long-lasting HW events. There is a spatiotemporal variation in the characteristics of HW among the THZ. Therefore, a more detailed understanding is required to study the causes of variability in each zone.

## 4 Discussion and conclusions

India is one of the main hot spots for severe heat waves, it is essential to understand the multiple aspects of heat waves on a regional scale to develop mitigation strategies. This study presents a comprehensive analysis of projected changes in the main characteristics of heat waves, namely intensity, frequency, duration, and spatial extent. The projected changes in the characteristics of the heat waves are quantified based on plausible emission scenarios SSP126, SSP245, SSP370 and SSP585 in different temperature homogeneous zones of India. Most of the studies on the projections consider all model ensembles for climate system analysis (Murari et al. 2015; Ntoumos et al. 2022; Perkins 2011; Hirsch et al. 2021). Here, we identify the reliable model(s) for a given metric in each temperature homogeneous zone considering the historical maximum temperature trends and the correlation of  $T_{\max}$  with the Niño 3.4 indexes. The selected models for each zone show a good approximation to the observed features. Accurate simulation of observed metrics such as trends and correlation is one of the primary measures of the reliability of future projections (Ramesh and Goswami 2014). Reliable projections of each THZ have a critical input for policy makers and decision support.

The characteristics of heat waves are analyzed in three periods, such as the near future, future, and far future. The results show that in the northern parts of India, the highest rate of increase in the  $T_{\max}$  anomaly is over the NW ( $0.41^{\circ}\text{C}/\text{decade}$ ) under SSP585. Heat wave days in the far future are likely to be longer in NW (16 days), which is more than the all-India average of 14 days. The projected change in the intensity of heat waves in NC is greater than that of the NW and all-India average. In NC, the intensity is expected to increase by about  $0.5^{\circ}\text{C}$  in the near future, and in the far future it will be more than  $1^{\circ}\text{C}$  under SSP585. The spatial extension of extreme ( $>11$  days) heat waves is expected to extend widely over the NW (14-fold) than the NC (8-fold) under the highest emission scenario, SSP585.

Currently least affected regions with heat waves are projected to be severe in the future like Peninsular India (Murari et al. 2015). When comparing the two coastal zones, WC and EC, projections show that the increasing trend in  $T_{\max}$  and the spatial extension of the higher range of  $T_{\max}$  are maximum in WC. The HW days and intensity of heat waves are projected to gradually increase in WC and EC. Warm days will intensify significantly over WC about 5.6 times under SSP585, and in EC it is 3.6 times. The findings suggest that by the end of the 21st century there will be a decrease in the occurrence of extreme HWs in the WC region; on the other hand, the total number of warm days (short-lived HW) will increase significantly. Extreme heat waves of more than 11 days are likely to have a greater spatial extent over WC, about 20 times, while over EC, it is about 4 to 8 times under SSP126 to SSP585. This study highlights that in WC, the characteristics of heat waves are not only increasing but accelerating under different climate change scenarios.

The intensity, frequency, duration, and area coverage of heat waves are projected to increase in IP, which is close to the average change in all India. In all THZ, the intensity of the heat waves will increase from the low emission scenario SSP126 to the high emission scenario SSP585. The projected intensity and frequency of the heat waves are likely to increase rapidly over WH and are least likely to increase over NE.

The results shows that the characteristics of the heat waves have a wide variation between the zones. For example, the NW is likely to have long and frequent heat waves, while coastal zones are projected to be more intense, and hence social and economic challenges vary from zone to zone. Therefore, this research highlights that it is vitally important to develop

region-specific mitigation strategies for each of the temperature-homogeneous zones in India. These projections of the characteristics of heat waves will be helpful for policy makers in managing regional climate risks and minimizing social risks.

In summary, the findings show that

- In the far future, projections under SSP370 show a severe increase in HW days over WH (24 days), NW (20 days) and IP (15 days), and the least over NE (11 days), where the all-India average is 17 days per season.
- In the far future, the highest increase ( $>3$ ) in the HW events will occur in parts of NW and WH under SSP370.
- The projected trend in HW days and events is relatively lower in coastal zones, but the trend in HW intensity is maximum ( $2.5^{\circ}\text{C}/\text{decade}$ ) in WC under the high-emission scenario. In the coastal zones, the projected change in intensity of heat waves is higher than in the other zones, which is  $1.75^{\circ}\text{C}$  under SSP585 and  $1.5^{\circ}\text{C}$  under SSP370 in the far future.
- The warm days are projected to increase about five-fold (52 days) over WC, and about three-fold (34–37 days) in EC, IP, WH and NW under SSP585. It suggests that by the end of the 21st century, there is a decrease in the occurrence of frequency of HW days in the WC region, on the contrary the total number of warm days will significantly increase
- The area of occurrence of extreme  $T_{\text{max}}$  of all THZ is significantly increasing under plausible scenarios. Under SSP585, the area of occurrence with  $T_{\text{max}}, >43^{\circ}\text{C}$  is most likely to increase to 16 fold over WC, 10 fold over EC, 1–3 fold over NW, NC, and IP, and the change will be less over WH and NE.
- The area of occurrence of extreme heat waves ( $>11$  days) is projected to increase 20-fold in WC under the SSP585 scenario and about 10-fold in NW, IP and EC at the end of the 21<sup>st</sup> century.

In the future, heat waves are projected to be more intense in the coastal zones and more frequent in the NW and WH, causing great social and economic challenges. Currently, the least affected WC is projected to have devastating changes in the characteristics of HW, especially the warm days are likely to get exacerbated in this zone. Tan et al. (2023) shows that the installation of cool roofs, green roofs, and solar panel roofs can reduce near-surface temperatures in urban areas. The severity of heat waves is amplified by the effect of urban heat islands (UHI), and increasing the tree canopy will reduce UHI, as well as heat-induced deaths (Chaston et al. 2022). The limitation of the study is that models that performed reasonably well in the historical period are assumed to be reliable for future projections. However, a more detailed and high-resolution study is needed to explore the causes of regional variability in the characteristics of projected heat waves.

**Supplementary Information** The online version contains supplementary material available at <https://doi.org/10.1007/s10584-023-03618-w>.

**Acknowledgements** The first author is acknowledging the Department of Science and Technology (DST), Government of India for the research fellowship under the Women Scientist Scheme WOS-A (SR/WOS-A/EA-33/2018)

**Author Contributions** Both authors have contributed to the conception and design of the study. Neethu C has done the data curation, investigation, visualization, and writing the original draft. Reviewing and editing the manuscript is done by K V Ramesh.

**Funding** The study was supported by the Department of Science and Technology (DST), funding under WOS -A (SR/WOS-A/EA-33/2018).

**Availability of data and materials** Bias-corrected CMIP6 data for South Asia is available at [https://zenodo.org/record/3987736#.YP\\_kp\\_nhVH5](https://zenodo.org/record/3987736#.YP_kp_nhVH5), CMIP6 models SST monthly data for the historical (1951–2014) period retrieved from the Earth System Grid Federation <https://esgf-node.ipsl.upmc.fr/search/cmip6-ipsl>. Observations Nino 3.4 index is obtained from [https://origin.cpc.ncep.noaa.gov/products/analysis\\_monitoring/ensostuff/ONI\\_v5.php](https://origin.cpc.ncep.noaa.gov/products/analysis_monitoring/ensostuff/ONI_v5.php).

**Code Availability** Not applicable

## Declarations

**Ethics approval** Not applicable

**Consent to participate** Not applicable

**Consent for publication** Not applicable

**Conflicts of interest** The authors declare that they have no known competing financial interests or personal relationships that could have appeared to influence the work reported in this paper.

## References

- Aadhar S, Mishra V (2019) A substantial rise in the area and population affected by dryness in South Asia under 1.5°C, 2.0°C and 2.5°C warmer worlds. *Environ Res Lett* 14(11):114,021. <https://doi.org/10.1088/1748-9326/ab4862>
- Ali H, Modi P, Mishra V (2019) Increased flood risk in Indian sub-continent under the warming climate. *Weather Clim Extrem* 25(100):212. <https://doi.org/10.1016/j.wace.2019.100212>
- Anderson GB, Bell ML (2011) Heat waves in the United States: mortality risk during heat waves and effect modification by heat wave characteristics in 43 US communities. *Environ Health Perspect* 119(2):210–218. <https://doi.org/10.1289/ehp.1002313>
- Bhattacharya A, Thomas A, Soni VK et al (2023) Opposite trends in heat waves and cold waves over India. *J Earth Syst Sci* 132(2):67. <https://doi.org/10.1007/s12040-023-02069-2>
- Cai W, Ng B, Wang G et al (2022) Increased ENSO sea surface temperature variability under four IPCC emission scenarios. *Nat Clim Change* 12(3):228–231. <https://doi.org/10.1038/s41558-022-01282-z>
- Chakraborty A, Seshasai M, Rao SK et al (2017) Geo-spatial analysis of temporal trends of temperature and its extremes over india using daily gridded (1 × 1) temperature data of 1969–2005. *Theor Appl Climatol* 130:133–149. <https://doi.org/10.1007/s00704-016-1869-8>
- Chakraborty D, Sehgal VK, Dhakar R et al (2019) Spatio-temporal trend in heat waves over India and its impact assessment on wheat crop. *Theor Appl Climatol* 138(3–4):1925–1937. <https://doi.org/10.1007/s00704-019-02939-0>
- Chaston TB, Broome RA, Cooper N et al (2022) Mortality burden of heatwaves in Sydney, Australia is exacerbated by the urban heat island and climate change: can tree cover help mitigate the health impacts? *Atmosphere* 13(5):1–13. <https://doi.org/10.3390/atmos13050714>
- Coates L, Haynes K, O'Brien J (2014) Exploring 167 years of vulnerability: an examination of extreme heat events in Australia 1844–2010. *Environ Sci Policy* 42:33–44. <https://doi.org/10.1016/j.envsci.2014.05.003>
- Das J, Umamahesh NV (2022) Heat wave magnitude over India under changing climate: projections from CMIP5 AND CMIP6 experiments. *Int J Climatol* 42(1):331–351. <https://doi.org/10.1002/joc.7246>
- Dash SK, Mangain A (2011) Changes in the frequency of different categories of temperature extremes in India. *J Appl Meteorol Climatol* 50(9):1842–1858. <https://doi.org/10.1175/2011JAMC2687.1>
- Delmotte M, Zhai VP, Pirani A, et al (2021) IPCC, 2021: summary for policymakers. in: *Climate change 2021: The physical science basis. contribution of working group i to the sixth assessment report of the intergovernmental panel on climate change*. Tech. rep., Cambridge, United Kingdom and New York, NY, USA, <https://doi.org/10.1017/9781009157896.001>
- Dube A, Singh H, Ashrit R (2021) Heat waves in India during mam 2019: verification of ensemble based probabilistic forecasts and impact of bias correction. *Atmos Res* 251(105):421. <https://doi.org/10.1016/j.atmosres.2020.105421>

- Dubey AK, Lal P, Kumar P et al (2021) Present and future projections of heatwave hazard-risk over India: a regional earth system model assessment. *Environ Res* 201(111):573. <https://doi.org/10.1016/j.envres.2021.111573>
- Eyring V, Bony S, Meehl GA et al (2016) Overview of the Coupled Model Intercomparison Project Phase 6 (CMIP6) experimental design and organization. *Geosci Model Dev* 9(5):1937–1958. <https://doi.org/10.5194/gmd-9-1937-2016>
- Ghatak D, Zaitchik B, Hain C et al (2017) The role of local heating in the 2015 Indian Heat Wave. *Sci Rep* 7(1):1–8. <https://doi.org/10.1038/s41598-017-07956-5>
- Hari V, Ghosh S, Zhang W et al (2022) Strong influence of North Pacific Ocean variability on Indian summer heatwaves. *Nature Commun* 13(1):1–11. <https://doi.org/10.1038/s41467-022-32942-5>
- Hirsch AL, Ridder NN, Perkins-Kirkpatrick SE et al (2021) CMIP6 multimodel evaluation of present-day heatwave attributes. *Geophys Res Lett* 48(22):1–11. <https://doi.org/10.1029/2021GL095161>
- Im ES, Pal JS, Eltahir EAB (2017) Deadly heat waves projected in the densely populated agricultural regions of South Asia. *Sci Adv* 3(8):e1603322. <https://doi.org/10.1126/sciadv.1603322>
- Jenamani, Jendrakumar (2012) Mausam. Analysis of ocean-atmospheric features associated with extreme temperature variation over east coast of India—a special emphasis to Orissa heat waves of 1998 and 2005 63(3):401–422. <https://doi.org/10.54302/mausam.v63i3.1231>
- Joshi MK, Rai A, Kulkarni A et al (2020) Assessing changes in characteristics of hot extremes over India in a warming environment and their driving mechanisms. *Sci Rep* 10(1):1–14. <https://doi.org/10.1038/s41598-020-59427-z>
- Koteswara Rao K, Lakshmi Kumar TV, Kulkarni A et al (2020) Projections of heat stress and associated work performance over India in response to global warming. *Sci Rep* 10(1):1–14. <https://doi.org/10.1038/s41598-020-73245-3>
- Kothawale DR, Rupa Kumar K (2005) On the recent changes in surface temperature trends over India. *Geophys Res Lett* 32(18):1–4. <https://doi.org/10.1029/2005GL023528>
- Kumar P, Sarthi PP (2019) Surface temperature evaluation and future projections over India using CMIP5 models. *Pure Appl Geophys* 176(11):5177–5201. <https://doi.org/10.1007/s00024-019-02203-6>
- Kumar S, Chanda K, Pasupuleti S (2023) Association of tropical daily precipitation extremes with physical covariates in a changing climate. *Stoch Environ Res Risk Assess* pp 1–19. <https://doi.org/10.1007/s00477-023-02433-0>
- Liu Z, Anderson B, Yan K et al (2017) Global and regional changes in exposure to extreme heat and the relative contributions of climate and population change. *Sci Rep* 7(1):1–9. <https://doi.org/10.1038/srep43909>
- Lu Y, Kueppers L (2015) Increased heat waves with loss of irrigation in the United States. *Environ Res Lett* 10(6). <https://doi.org/10.1088/1748-9326/10/6/064010>
- Madhu S, Kumar TL, Barbosa H et al (2015) Trend analysis of evapotranspiration and its response to droughts over India. *Theor Appl Climatol* 121:41–51. <https://doi.org/10.1007/s00704-014-1210-3>
- Malik P, Bhardwaj P, Singh O (2021) Heat wave fatalities over India: 1978–2014. *Current Sci* 120(10):1593–1599. <https://doi.org/10.18520/cs/v120/i10/1593-1599>
- Mandal R, Joseph S, Sahai AK et al (2019) Real time extended range prediction of heat waves over India. *Sci Rep* 9(1):1–11. <https://doi.org/10.1038/s41598-019-45430-6>
- Mazdiyasi O, AghaKouchak A, Davis SJ et al (2017) Increasing probability of mortality during Indian heat waves. *Sci Adv* 3(6):1–6. <https://doi.org/10.1126/sciadv.1700066>
- Meehl GA, Tebaldi C (2004) More intense, more frequent, and longer lasting heat waves in the 21st century. *Science* 305(5686):994–997. <https://doi.org/10.1126/science.1098704>
- Mishra V, Bhatia U, Tiwari AD (2020) Bias-corrected climate projections for South Asia from Coupled Model Intercomparison Project-6. *Sci Data* 7(1):1–13. <https://doi.org/10.1038/s41597-020-00681-1>
- Mitchell D, Heaviside C, Vardoulakis S et al (2016) Attributing human mortality during extreme heat waves to anthropogenic climate change. *Environ Res Lett* 11(7):074,006. <https://doi.org/10.1088/1748-9326/11/7/074006>
- Mukherjee S, Mishra V (2018) A sixfold rise in concurrent day and night-time heatwaves in India under 2°C warming. *Sci Rep* 8(1):1–9. <https://doi.org/10.1038/s41598-018-35348-w>
- Murari KK, Ghosh S, Patwardhan A et al (2015) Intensification of future severe heat waves in India and their effect on heat stress and mortality. *Reg Environ Change* 15:569–579. <https://doi.org/10.1007/s10113-014-0660-6>
- Murari KK, Sahana AS, Daly E et al (2016) The influence of the El Niño Southern Oscillation on heat waves in India. *Meteorol Appl* 23(4):705–713. <https://doi.org/10.1002/met.1594>
- Nandi S, Swain S (2022) Analysis of heatwave characteristics under climate change over three highly populated cities of South India: a CMIP6-based assessment. *Environ Sci Pollut Res* pp 1–13. <https://doi.org/10.1007/s11356-022-22398-x>



- Naveena N, Satyanarayana GC, Rao KK, et al (2021) Heat wave characteristics over India during ENSO events. *J Earth Syst Sci* 130(3). <https://doi.org/10.1007/s12040-021-01674-3>
- Neethu C, Ramesh KV (2022) High-resolution spatiotemporal variability of heat wave impacts quantified by thermal indices. *Theor Appl Climatol* 148(3–4):1181–1198. <https://doi.org/10.1007/s00704-022-03987-9>
- Neethu C, Ramesh KV, Shafeer KB (2020) Understanding the spatio-temporal structure of recent heat waves over India. *Nat Hazards* 102(2):673–688. <https://doi.org/10.1007/s11069-019-03593-5>
- Ntoumos A, Hadjinicolaou P, Zittis G et al (2022) Projected air temperature extremes and maximum heat conditions over the Middle-East-North Africa (MENA) region. *Earth Syst Environ* 6(2):343–359. <https://doi.org/10.1007/s41748-022-00297-y>
- Panda DK, AghaKouchak A, Ambast SK (2017) Increasing heat waves and warm spells in India, observed from a multispect framework. *J Geophys Res* 122(7):3837–3858. <https://doi.org/10.1002/2016JD026292>
- Pattanaik DR, Mohapatra M, Srivastava AK et al (2017) Heat wave over India during summer 2015: an assessment of real time extended range forecast. *Meteorol Atmos Phys* 129(4):375–393. <https://doi.org/10.1007/s00703-016-0469-6>
- Perkins SE (2011) Biases and model agreement in projections of climate extremes over the tropical Pacific. *Earth Interact* 15(24):1–36. <https://doi.org/10.1175/2011EI395.1>
- Perkins SE, Alexander LV, Nairn JR (2012) Increasing frequency, intensity and duration of observed global heatwaves and warm spells. *Geophys Res Lett* 39(20):1–5. <https://doi.org/10.1029/2012GL053361>
- Perkins-Kirkpatrick S, Lewis S (2020) Increasing trends in regional heatwaves. *Nature Commun* 11(1):1–8. <https://doi.org/10.1038/s41467-020-16970-7>
- Purnadurga G, Kumar T, Kundeti K et al (2017) Investigation of temperature changes over india in association with meteorological parameters in a warming climate. *Int J Climatol* 38. <https://doi.org/10.1002/joc.5216>
- Ramesh KV, Goswami P (2014) Assessing reliability of regional climate projections: the case of Indian monsoon. *Sci Rep* 4(1):1–9. <https://doi.org/10.1038/srep04071>
- Rao CS, Gopinath K, Prasad J et al (2016) Climate resilient villages for sustainable food security in tropical India: concept, process, technologies, institutions, and impacts. *Adv Agron* 140:101–214. <https://doi.org/10.1016/bs.agron.2016.06.003>
- Rao KK, Reddy PJ, Chowdary JS (2023) Indian heatwaves in a future climate with varying hazard thresholds. *Environ Res Clim*. <https://doi.org/10.1088/2752-5295/acb077>
- Ratnam JV, Behera SK, Ratna SB et al (2016) Anatomy of Indian heatwaves. *Sci Rep* 6:1–11. <https://doi.org/10.1038/srep24395>
- Ray K, Giri R, Ray S et al (2021) An assessment of long-term changes in mortalities due to extreme weather events in India: a study of 50 years' data, 1970–2019. *Weather Clim Extremes* 32(100):315. <https://doi.org/10.1016/j.wace.2021.100315>
- Rohini P, Rajeevan M, Srivastava A (2016) On the variability and increasing trends of heat waves over India. *Sci Rep* 6(1):1–9. <https://doi.org/10.1038/srep26153>
- Rohini P, Rajeevan M, Mukhopadhyay P (2019) Future projections of heat waves over India from CMIP5 models. *Clim Dynamics* 53(1):975–988. <https://doi.org/10.1007/s00382-019-04700-9>
- Ross RS, Krishnamurti T, Pattanaik S et al (2018) Decadal surface temperature trends in India based on a new high-resolution data set. *Sci Rep* 8(1):7452. <https://doi.org/10.1038/s41598-018-25347-2>
- Russo S, Dosio A, Graversen RG et al (2014) Magnitude of extreme heat waves in present climate and their projection in a warming world. *J Geophys Res Atmos* 119(22):12–500. <https://doi.org/10.1002/2014JD022098>
- Shah R, Mishra V (2014) Evaluation of the reanalysis products for the monsoon season droughts in India. *J Hydrometeorol* 15(4):1575–1591. <https://doi.org/10.1175/JHM-D-13-0103.1>
- Shetty S, Umesh P, Shetty A (2023) Future transition in climate extremes over Western Ghats of India based on CMIP6 models. *Environ Monit Assess* 195(5):578. <https://doi.org/10.1007/s10661-023-11090-3>
- Spinoni J et al (2020) Future global meteorological drought hot spots: a study based on CORDEX data. *J Clim* 33(9):3635–3661. <https://doi.org/10.1175/JCLI-D-19-0084.1>
- Srivastava AK, Rajeevan M, Kshirsagar SR (2009) Development of a high resolution daily gridded temperature data set (1969–2005) for the Indian region. *Atmos Sci Lett* 10(4):249–254. <https://doi.org/10.1002/asl.232>
- Stott PA, Stone DA, Allen MR (2004) Human contribution to the European heatwave of 2003. *Nature* 432(7017):610–614. <https://doi.org/10.1038/nature03089>
- Tan H, Kotamarthi R, Wang J et al (2023) Impact of different roofing mitigation strategies on near-surface temperature and energy consumption over the Chicago metropolitan area during a heatwave event. *Sci Total Environ* 860(160):508. <https://doi.org/10.1016/j.scitotenv.2022.160508>
- Vittal H, Villarini G, Zhang W (2020) On the role of the Atlantic ocean in exacerbating Indian heat waves. *Clim Dynamics* 54(3–4):1887–1896. <https://doi.org/10.1007/s00382-019-05093-5>

- Zhang X, Alexander L, Hegerl GC et al (2011) Indices for monitoring changes in extremes based on daily temperature and precipitation data. *Wiley Interdiscip Rev Clim Change* 2(6):851–870. <https://doi.org/10.1002/wcc.147>
- Zhu X, Wei Z, Dong W et al (2020) Dynamical downscaling simulation and projection for mean and extreme temperature and precipitation over Central Asia. *Clim Change* 54(7):3279–3306. <https://doi.org/10.1007/s00382-020-05170-0>

**Publisher's Note** Springer Nature remains neutral with regard to jurisdictional claims in published maps and institutional affiliations.

Springer Nature or its licensor (e.g. a society or other partner) holds exclusive rights to this article under a publishing agreement with the author(s) or other rightsholder(s); author self-archiving of the accepted manuscript version of this article is solely governed by the terms of such publishing agreement and applicable law.